

REFINING OF NIOBIUM CONCENTRATE BY CARBOTHERMIC REDUCTION¹

João Batista Ferreira Neto²

Cyro Takano³

Flávio Beneduce Neto²

Abstract

Ferro Niobium is produced by aluminothermic reduction of the niobium concentrate. However, the niobium concentrate has impurities, such as phosphorus, lead and tin, which can contaminate the Ferro Niobium. Therefore, the niobium concentrate must be refined before aluminothermy. In the present work, the carbothermic reduction of niobium concentrate was investigated as a method to promote the impurities removal. The carbothermic reduction of niobium concentrate was investigated in self-reducing briquettes in temperatures between 1100 and 1250°C, aiming to promote the reduction of impurities, mainly phosphorus. The reduction was carried out using graphite as carbonaceous material. The reduction was evaluated by gas volume generated during the experiments with self-reducing briquettes. After reduction, the briquettes were evaluated in scanning electronic microscope. It was observed that the iron oxide of the niobium concentrate was simultaneously reduced with oxides of phosphorus, lead and tin, producing an alloy Fe-Sn-P, with phosphorus content up to 20%. The best fitting with the experimental results was obtained with the first-order kinetic expression. Based on the results with graphite -325 mesh, it was obtained an apparent activation energy of 296,3 +/- 29 kJ/mol. It was also observed a significant effect of particle size of graphite on the reaction rate.

Key notes: Ferro niobium; Niobium.

REFINO DE CONCENTRADO DE NIÓBIO POR MEIO DE REDUÇÃO CARBOTÉRMICA

Resumo

Ferro Nióbio é produzido por redução aluminotérmica de concentrado de nióbio. Contudo, o concentrado de nióbio tem impurezas, tais como fósforo, chumbo e estanho, as quais podem contaminar a liga Ferro Nióbio. Desta forma, o concentrado de nióbio deve ser refinado antes a aluminotermia. No presente trabalho, a redução carbotérmica de concentrado de nióbio foi investigada como um método para promover a remoção de suas impurezas. A redução carbotérmica do concentrado de nióbio foi investigada em briquetes auto-redutores em temperaturas entre 1100 e 1250°C, objetivando promover a redução das impurezas do concentrado, principalmente o fósforo. A redução foi realizada usando grafite como material redutor. A redução foi avaliada pelo volume de gás gerado nos experimentos. Após a redução os briquetes foram caracterizados por Microscopia Eletrônica de Varredura. Observou-se que os óxidos de ferro do concentrado de nióbio foram simultaneamente reduzidos com os óxidos contendo fósforo, chumbo e estanho, produzindo uma liga Fe-P-Sn, com teor de fósforo de até 20%. O melhor ajuste com os resultados experimentais foi obtido com a expressão cinética de 1ª ordem. Baseado nos resultados empregando grafite - 325 mesh como agente redutor foi obtida uma energia de ativação aparente de 296,3 +/- 29 kJ/mol. Foi observado também um importante efeito do tamanho de partícula da grafita na velocidade de redução.

Palavras-chave: Ferro nióbio; Nióbio

¹ *Technical contribution to the 7th Japan-Brazil Symposium on Dust Processin-Energy-Environment in Metallurgical Industries and 1st International Seminar on Self-reducing and Cold Bold Agglomeration, September 8-10 2008, São Paulo City – São Paulo State – Brazil*

² Metallurgy and Ceramic Materials Laboratory. Processes and Products Technology Center. Institute for Technological Research. Av. Prof. Almeida Prado, 532. Sao Paulo, Brazil. jbfnet@ipt.br; fbene@ipt.br

³ Metallurgical and Materials Engineering Department of the Escola Politecnica. University of Sao Paulo. Av. Prof. Mello Moraes, 2463. Sao Paulo, Brazil. cytakano@usp.br

1 INTRODUCTION

More than 75% of Niobium is applied in microalloyed steels production, with Nb content between 0,02 and 0,04%. It is also currently used in heat resistance stainless steels (~1%Nb) and in superalloys (~5% Nb) used in aircraft and stationary turbines. Both applications represent, respectively, approximately 12% and 10% of all Nb consumed in the world. In the steel industry, Nb is added as Fe-Nb, with approximately 65%Nb. The main Nb producers in the world are CBMM (Brazil), NIOBEC (Canada) and Mineração Catalão (Brazil) of Anglo American group. The Fe-Nb consumption is estimated as 35.000 t/y.

Fe-Nb is produced by aluminothermy of a Niobium Concentrate. Therefore, the concentrate must be as pure as possible in order to prevent transferring of impurities to Fe-Nb. Consequently, the concentrate must be refined before aluminothermy.

One of the most feasible alternatives for impurities removal from Nb concentrate is to promote a selective carbothermic reduction of the Nb concentrate in a first step, followed by a melting step. During the first step, the impurities would be selectively reduced, forming a metallic phase, at same time that the niobium oxide of concentrate would be preserved. During the second step, the metallic phase, rich in impurities, would be separated by melting from the refined niobium concentrate. Since 2000, CBMM has adopted a similar process for Nb concentrate refining⁽¹⁾, replacing a leaching plant by a pyrometallurgical plant.

The present work presents a fundamental study of the carbothermic reduction of the CBMM's niobium concentrate.

2 MATERIALS AND METHODS

2.1 Niobium Concentrate

The carbothermic reduction experiments were carried out using CBMM's niobium concentrate after 2 h calcination at 1000°C.

Table 1 shows the chemical composition of the calcined concentrate.

Table 1. Chemical composition of calcined Niobium Concentrate.

%									
Pb	Ta ₂ O ₅	Nb ₂ O ₅	P	TiO ₂	SiO ₂	Fe ₂ O ₃	S	C	Sn
0,54	0,23	59,0	0,89	3,92	1,00	5,95	0,039	0,002	0,1

Particle distribution of the concentrate presented 80% < 75 μm and 43% < 44 μm.

Samples of Niobium concentrate before and after calcination were characterized by SEM and X-ray diffraction. The complete results⁽²⁾ will be present in the future. A summary of the results is presented below:

- Main source of **Nb**: Bariopyrochlore (Ba_{0.33}Nb_{1.78}O₆.H₂O) after calcination.
- Main source of **Fe**: Free porous iron oxides; pseudorutile/Ilmenite; complex iron oxides with Nb, Ba and Ti (from interaction between iron oxides and bariopyrochlore particles).
- Main source of **P**: porous particles rich in P and Al. Probably from Gorceixite mineral [Ba,Ce(Al,Fe)₃(PO₄)₂(OH)₅.H₂O] after calcination.
- Main source of **Pb**: Probably plumbopyrochlore [Pb_xNb_yO₆(OH).H₂O] after calcination.

2.2 Self-reducing Briquettes Preparation

Briquettes were prepared by pressing a mixture between calcined concentrate and 1,86%C as graphite (-325 mesh and in the range between -150 and 270 mesh). The analysis of graphite is presented in Table 2.

Table 2. Analysis of graphite.

		(%)		
Humidity	Ash	S	VM*	Fixed C
< 0,01	< 0,1	< 0,1	1,5	98,5

*Volatile matter

The amount of carbon in briquettes was calculated to reduce totally PbO , SnO_2 , P_2O_5 and partially Fe_2O_3 (up to 1,6% Fe_2O_3). The reason for considering a partial Fe reduction was based on previous experiments of the smelting of niobium concentrate, which showed an excessive Nb reduction when the Fe_2O_3 content was lower than 1,6%.

Briquettes (7,1 mm diameter x 25 mm height) with approximately 3,1 g of mixture (dry basis) were compacted at 375 MPa using only water (10%). The water was added to get enough green strength for handling. Before reducing experiments the water was removed by drying.

2.2 Determination of Reacted Fraction

The Figure 1 shows the scheme of experimental apparatus adopted for kinetic measurements.

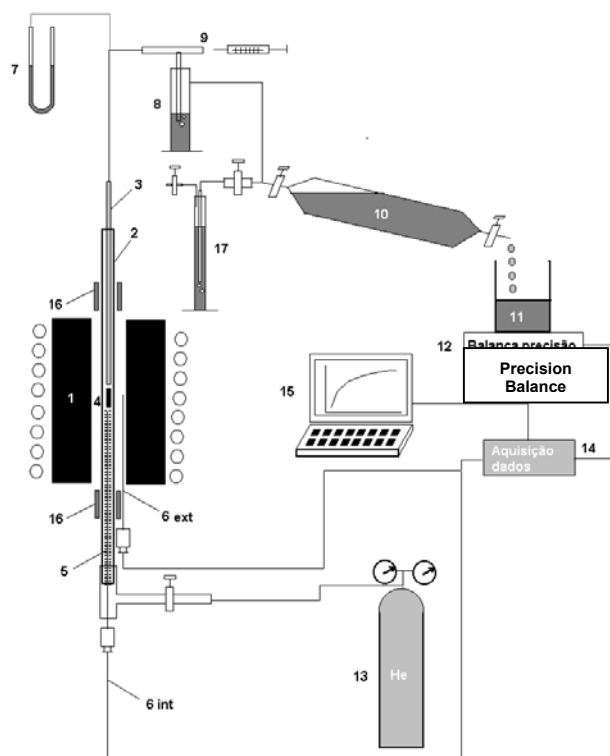


Figure 1. Experimental apparatus. 1. Resistance Furnace, 2. Quartz tube ($\phi_{int} = 10$ mm, $h = 1000$ mm); 3. Alumina tube ($\phi_{int} = 4$ holes of 1,5 mm each x $\phi_{ext} = 6$ mm); 4. Briquette ($\phi = 7,1$ mm, $h \sim 25$ mm); 5. Alumina particles; 6. K thermocouples (ext – external thermocouple; int – internal thermocouple); 7. “U” tube for pressure controlling; 8. Liquid seal; 9. “T” for gas sampling; 10. Gas ampoule (full of liquid at the initial instant); 11. Beaker. 12. Electronic balance; 13. Helium (99,999%); 14. Data acquisition system; 15. Computer; 16. Water cooled case; 17. Graduated cylinder for He pressure releasing before starting the reduction.

The reaction rate was determined by measuring the gas volume generated as a function of time during the experiments. Therefore, a gas sealed system has been constructed, in order to keep the “dead” volume as small as possible avoiding any dilution of the reducing gas by He used to purge the reaction chamber (quartz tube). In addition, the reaction chamber had a diameter close to the diameter of the briquette, in order to decrease the time to reach isothermal conditions. The reaction chamber was quickly moved to the hot zone of the furnace, promoting a fast heating up of the briquette.

The experiment started with the briquette in the cold zone (16) while the furnace was heat up to the required temperature. During this period, the quartz tube (2) was purged with He, which is removed through the liquid seal (17). When the furnace reached the required temperature, the quartz tube (2) was moved to the position (4), at same time that the reference temperature of the power control system was changed from external thermocouple (6 ext) to the internal thermocouple (6 int), in order to heat up the briquette as fast as possible, and to promote a more accuracy control of the temperature of the briquette. During this period, the gas valves of the ampoule (10) were opened and the outlet of the liquid seal (17) was closed. The gas generated during reduction was collected in the ampoule (10) replacing its liquid solution, which was transferred to a beaker (11) continuously weighted by electronic balance (12) connected to an acquisition data system (14), which transfer the data to a computer (15). Therefore, the gas volume generated during the experiment is indirectly determined by the liquid weight dislocated from the ampoule. In some experiments, gas samples were collected in the position (9), where a liquid seal (8) allowed the sampling of gas, free of the gas accumulated in the ampoule (10). These samples were analyzed by gas chromatography. A complete description of the experimental apparatus has been presented elsewhere.⁽²⁾

Table 3 shows the distribution of the maximum gas volume expected (CO+CO₂) according to reduced oxides.

Table 3. Expected volume of CO-CO₂ (STP cm³) by gram of concentrate according to impurities reduced.

Element/compound	% in concentrate	%Expected concentrate after reduction	CO/CO ₂ (STP cm ³)/g concentrate	Expected volumetric gas distribution (%)
Fe ₂ O ₃	5,95	1,6	18,3	51,8
P (P ₂ O ₅)	0,89	0	16,0	45,3
Pb (PbO)	0,54	0	0,6	1,7
Sn (SnO ₂)	0,10	0	0,4	1,1
Total	7,48	1,6	35,3	100

Admitting the gas generated as a CO/CO₂ mixture only, the reacted fraction of carbon can be calculated by the gas volume (STP) generated during the reduction, independently of the gas chemical composition, as given by expression:

$$f_C = (M_{C,t})/(M_{C,max})$$

Where:

f_C – Reacted Fraction of Carbon

$M_{C,t}$ – Carbon weight accumulated in generated gas in time t (weight of reacted carbon) (g)

$M_{C,max}$ – Maximum expected Carbon weight in the gas, corresponding to 1,86%C in the mixture, or 0,0189 g of carbon for each gram of concentrate.

$$M_C (g) = \text{Gas volume STP cm}^3 * (12/22.400)$$

3 RESULTS AND DISCUSSION

3.1 Effect of Temperature

The effect of temperature was evaluated mainly in experiments carried out with graphite -325 mesh. Figure 2 shows the effect of temperature on the reacted fraction of carbon.

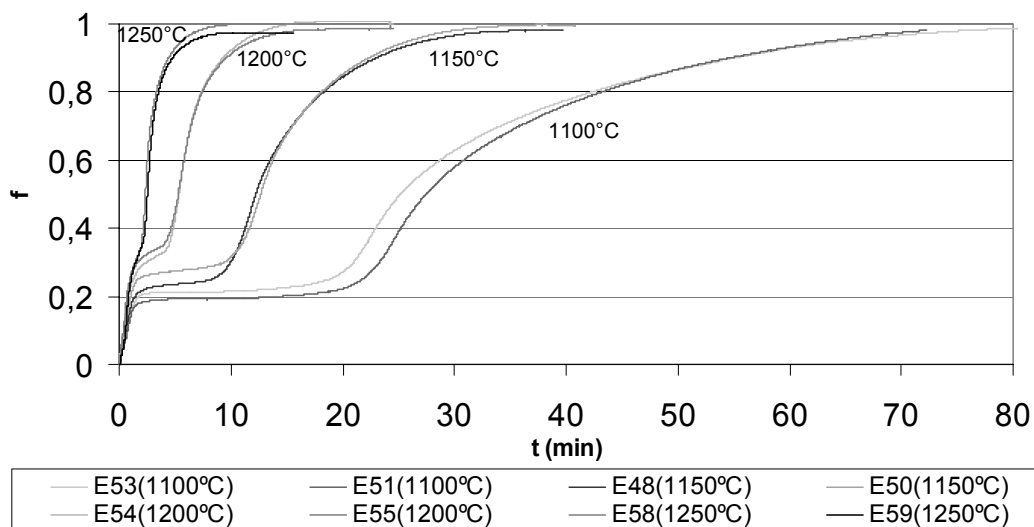


Figure 2. Effect of temperature on the reacted fraction of carbon (f) during experiments with graphite < 325 mesh.

Figure 2 shows that the temperature has a significant effect on the reaction rate. This fact indicates that the chemical reactions have an important role on the global kinetic of the process. One can be also observe that the whole carbon of the sample was reacted, since the gas generation stops after a certain period of time, which is longer in lower temperatures. In addition, the gas volume produced at the end of the experiments, at different temperatures, was closed to that estimated in table 2 (35,3 STPcm³/g concentrate).

In this figure, one can be also observe a step where the reduction rate was very slow. This step, called *induction period*, was longer at low temperature. However, it tended to disappear in experiments carried out at higher temperatures, for instance 1250°C. The reduction curves can be divided in four steps:

Initial step: Characterized by fast gas generation, from 0,8 min (1250°C) to 1,4 min (1100°C). It means that most of this period occurred under non-isothermal condition, based on the recorded temperature of thermocouple (6 int), described in detail in reference (2).

Induction step: Characterized by very slow reduction rate, with few gas generation. This step was strongly affected by temperature.

Acceleration step: Characterized by fast increasing of gas volume as well as by a strong effect of the temperature. Main step of the reduction (higher quantity of gas generated).

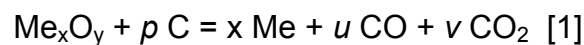
Slowdown step: Final period of the reduction, where the reduction rate decreased quickly, caused by reducing agent consumption.

As shown in Table 2, the gas volume estimated for tin and lead reduction was lower than 3% of the total expected volume (approximately 1 STPcm³/g concentrate). Therefore, considering that only the Fe, Pb, Sn and P oxides of the concentrate were reduced, one can conclude that those curves show almost exclusively the Fe and P reduction.

A brief discussion of phenomena that could be occurring during these steps will be presented as followed. Some conclusions have been supported by EDS analysis of samples of interrupted experiments at the end of these steps.

Initial step:

Briquettes evaluated at the end of this step did not show any detectable metallic phase, even Pb or Sn. Based on the gas volume generated in this step, higher than the volume generated for PbO and SnO₂ reductions, one might certainly conclude that there is an effect of the reduction of iron and/or phosphorus oxides on this period. Admitting a reduction from Fe³⁺ to Fe²⁺, would be generated approximately *4,61 STPcm³ of gas per gram of concentrate. This volume was calculated based on Boudouard controlling step, which means CO/CO₂ ratios are close to the equilibrium ratios Fe₂O₃/Fe₃O₄ and Fe₃O₄/FeO, as following:



This volume is relatively close to that observed in this step (6 to 9 STPcm³/g concentrate). Some difference could be explained by some P₂O₅ reduction or Nb₂O₅ reduction to sub-oxides (mainly NbO₂). However, the reduction of P without Fe presence or the reduction from Nb₂O₅ to NbO₂ are slow⁽²⁾, with a small contribution to the gas volume generated in this step. The fact that neither Pb nor Sn were found at the end of this step, can be explained by low activities of their oxides in the Nb compounds.

Induction step:

The characterization of briquettes of interrupted experiments at the end of the induction step showed the formation of the first nuclei of metallic phases, which consist of lead particles precipitated on phases rich in Pb and Nb (Plumbopyrochlore), and some particles of iron with high phosphorous and tin content, as shown in Figure 3.

Table 3 shows the EDS chemical compositions of the particles presented in Figure 3. The small size of lead particles [spherical white particles shown in Figure 3(a)] caused an interference on EDS chemical analysis. However, their high Pb content and their spherical shape indicate that those particles are reduced Pb oxide. The Figure 3(b) shows an oxide of Fe and Ti with two metallic particles of Fe-P-Sn. The high Sn content, higher than Sn content of the FeP particles in the later steps, shows that this element was reduced preferentially in earlier steps.

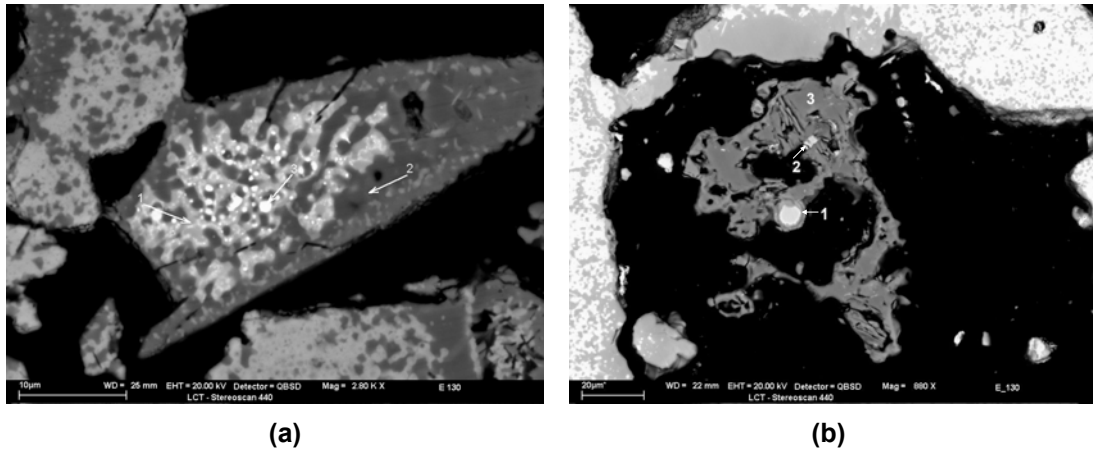


Figure 3. SEM-BSE image of polished section of a briquette of an interrupted experiment at the end of induction step. **(a)** 1- oxide rich in Nb, Pb and Ba; 2- oxide rich in Nb and Fe and 3- particles of Pb; **(b)** 1 and 2 – particles of Fe-P-Sn and 3- oxide of Fe, Ti and Nb.

Table 3. EDS analysis of particles shown in figure 3 (in %).

Identification	Nb	Fe	Ti	Ba	Pb	Sn	P	O
Figure 3(a)								
1	45,6	1,2	-	20,5	9,3	-	-	23,4
2	55,0	14,0	-	1,8	-	-	-	25,2
3 (metallic particles)	14,4	2,9	-	3,5	59,7	1,7	-	17,9
Figure 3(b)								
1(metallic particle)	-	83,2	-	-	-	10,1	6,7	-
2(metallic particle)	-	83,6	-	-	-	5,0	11,4	-
3 (Fe-Ti-Nb-O)	7,9	35,6	25,1	-	-	-	-	31,5

Chemical compositions of gas samples collected during the initial and induction steps showed an increasing of CO/CO₂ ratio from Fe₃O₄/FeO to FeO/Fe equilibrium,⁽²⁾ suggesting Boudouard reaction controll. One can conclude that the induction step is characterized by a nucleation period, where the first metallic nuclei are formed, enhancing the Boudouard reaction rate in the next step (acceleration), when the Boudouard reaction would be catalyzed.⁽³⁻⁶⁾

Mourão et al.⁽³⁾ and Ajersch⁽⁷⁾ observed a similar behavior, consisting in a step of low reaction rate followed by a acceleration step during a reduction of self-reducing pellets of iron ore. Both concluded that the Boudouard reaction was catalyzed by the iron particles nucleation. Mourão et al.⁽³⁾ observed this effect only at low temperatures and when the experiments were carried out without the presence of an inert gas, and in experiments using coke as reductant, which is a reducing agent with low reactivity. This fact supports the hypotheses of Boudouard controlling, since it is enhanced by low temperatures and by low reactive reducing agents. This induction period was also observed by Gupta et al.⁽⁸⁾ during ilmenite reduction with graphite. They observed that this period was shorter at high temperatures and it was almost eliminated in presence of iron particles, as catalyst agent.

The iron nuclei also apparently improve the P and Sn oxides reduction, since their activities are decreased by Fe.

Acceleration Step:

This step is characterized by increasing of the reaction rate and by increasing of the number of nuclei of particles of metallic iron. This step was also strongly affected by temperature.

Figure 4 shows optical images of briquettes of experiments carried out at 1150°C, interrupted at 18 minutes (fraction reacted ~0,8). This figure shows several metallic particles, many of them with spherical shape. It can also be observed a larger density of metallic particles in some regions. These regions were identified by EDS as iron and titanium oxides or iron, titanium, niobium oxides.

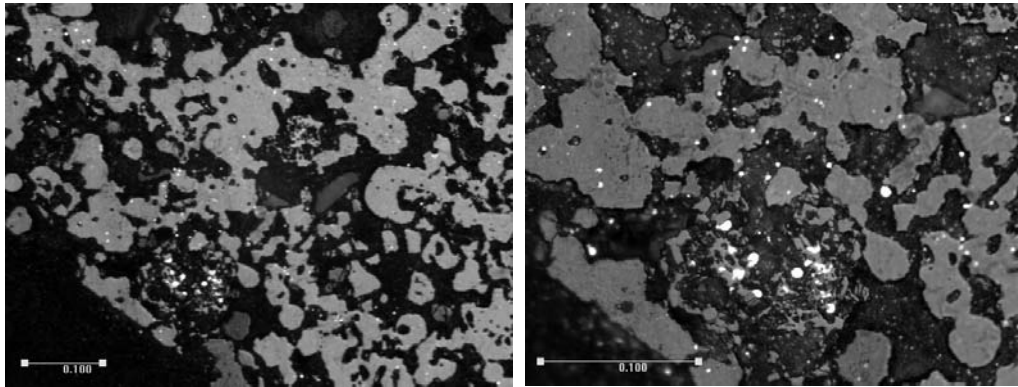


Figure 4. Optical images of a briquette of a experiment carried out at 1150°C, interrupted at 18 minutes (fraction reacted ~0,8). Reference in mm.

Figure 5 shows BSD images of some regions or particles observed in this interrupted experiment.

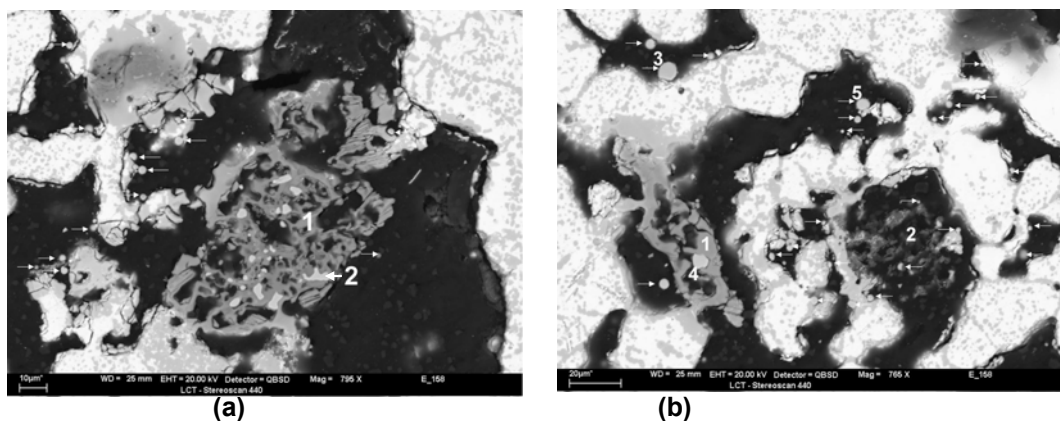


Figure 5. BSD images of briquette of an experiment carried out at 1150°C, interrupted at 18 minutes, on the acceleration step. **(a)** - 1 – particle of Fe, Ti, Nb oxide after reduction, showing several particles of metallic phase (2 and arrows). **(b)** – 1- particle of Fe, Ti, Nb oxide after reduction, showing particles of metallic phase (3,4 and 5 and arrows); 2- aluminum oxide and several metallic particles (arrows).

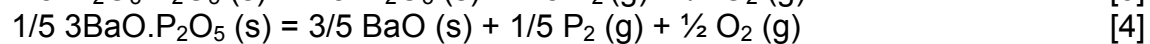
Table 4 presents the EDS chemical compositions of the oxides and metallic particles shown in figure 5. This table shows that most of metallic particles are Fe-P alloy with Sn content lower than that observed in iron particles analyzed in the induction period. The particles indentified as 1 in Figures 5(a) and 5(b) are oxides rich in Ti and Nb and with low Fe content. They probably were Fe-Ti-Nb oxides before reduction. These oxides were sources of iron to produce the Fe-P particles.

Table 4. Quantitative analysis (EDS) of particles shown in figure 5 (% in weight).

Identification	Nb	Fe	Ti	Al	Sn	P	O
Figure 5(a)							
2(Fe-P)	1,2	83,8	-	-	0,98	14,0	-
Arrow (Fe-P)	1,9	82,4	-	-	1,0	14,7	-
Arrow (Fe-P)	-	87,0	-	-	-	12,1	-
Arrow (Fe-P)	2,9	80,8	-	-	1,1	15,3	-
Arrow (Fe-P)	2,5	82,8	-	-	1,4	13,3	-
1 partially reduced Fe-Ti-Nb oxide	9,7	0,6	49,9	-	-	-	39,8
Figure 5(b)							
1 partially reduced Fe-Ti-Nb oxide	24,2	0,7	38,3	-	-	-	36,7
2 partially reduced Al-P oxide	1,7	2,1	-	53,2	-	-	42,2
3 (Fe-P)	3,8	74,3	-	-	-	22,2	-
4 (Fe-P)	-	85,6	-	-	1,2	12,0	-
5 (Fe-P)	-	85,1	-	-	1,4	11,5	-

It also can be observed that regions of calcined concentrate, rich in P, Al (probably gorceixite mineral after calcinations⁽²⁾) were transformed in a region rich only with aluminum and oxygen (probably aluminum oxide), as shown in Figure 5(b) (region 2). Based on high phosphorus content in metallic particles can be concluded that the source of P was a phosphate with low thermodynamic stability, probably an aluminum phosphate, as shown in the thermodynamic evaluation presented below. This fact also agrees with the high level of Al and P and low level of Ba found in the phosphorus rich regions of the niobium concentrate after calcination.

The relative stability of some phosphates can be evaluated as a function of P_2 ¹ partial pressure, as well as, a function of CO/CO₂ ratio at constant temperature and pressure ($p_{CO}+p_{CO_2} = 1 \text{ atm}$), as shown by reactions below:



This graphic representation is presented in Figure 6. In this same figure is presented the Boudouard equilibrium.

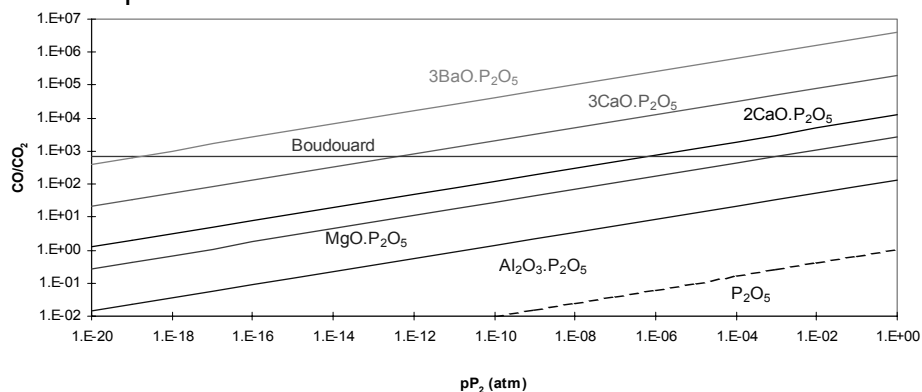


Figure 6. Relationship between CO/CO₂ equilibrium ratio and P₂ partial pressure (atm) for some phosphates at 1150°C. It is also presented the Boudouard equilibrium ($p_{CO}+p_{CO_2} = 1 \text{ atm}$).

¹ Based on calculations made previously⁽²⁾, it was defined P₂ as the main specie in the gas phase in equilibrium with Fe-P (up to 20%P).

Figure 6 shows that the P_2 partial pressure increases with increasing of CO/CO_2 ratio and that it is higher for less stable phosphates. It is not presented in this figure, however it has been previously⁽²⁾ verified, that higher temperatures enhance the increasing of P_2 partial pressure.

On the other hand, phosphorus can dissolve easily in iron, as shown by reaction below:



Figure 7(a) shows the calculated equilibrium of phosphorus content in Fe as a function of P_2 partial pressure (atm). In the Figure 7(b) is shown, as reference, the Fe-P phase diagram.

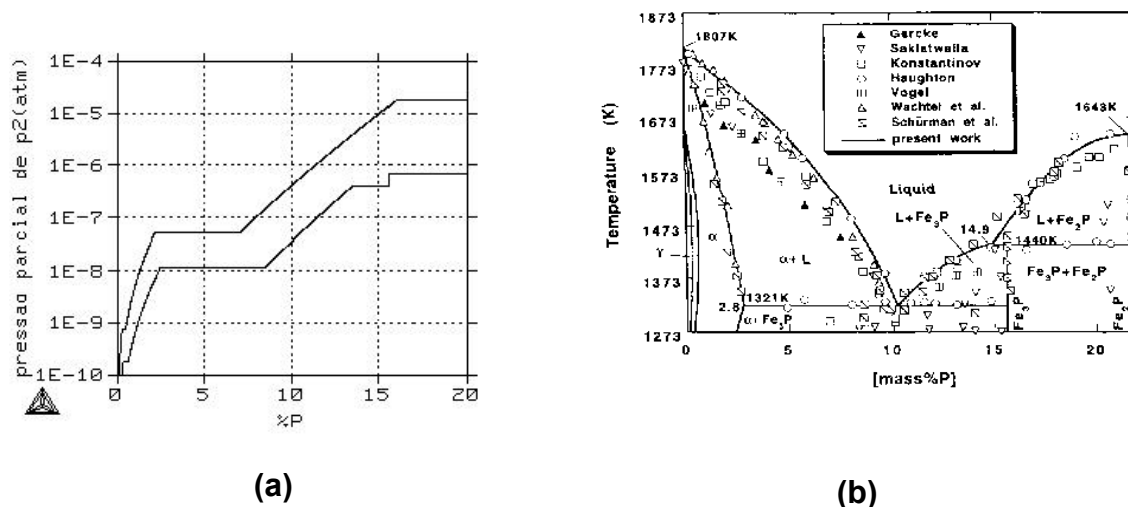


Figure 7. (a) Equilibrium of P content in iron as a function of partial pressure of P_2 at 1150°C (inferior curve) and 1250°C (superior curve). **(b)** Fe-P phase diagram⁽⁹⁾.

The dwells observed in Figure 7(a) at 1250°C consist in, respectively, equilibrium (γ - α), (α - liquid) and (liquid- Fe_2P).

Observing Figures 6 and 7(a), it can be verified that even low P_2 partial pressures will result in high phosphorus content in iron. For example, to reach the Fe_2P -liquid dwell of the Figure 7(a) at 1150°C, meaning more than 15% of phosphorus, a P_2 partial pressure as low as 10^{-6} atm is enough.

Considering the reduction with CO/CO_2 , it can be verified in the Figure 6 that this P_2 partial pressure is reached with a CO/CO_2 ratio between 1 and 10 for aluminum phosphate reduction, while it would be impossible reach this pressure for barium phosphate reduction, because it would be necessary ratios CO/CO_2 higher than Boudouard.

Therefore, one can be concluded that the source of P of Fe-P particles is the P_2 gas. This gas was generated by reduction of an aluminum phosphate produced by the calcination of gorceixite of the niobium concentrate.

Based on the expected reduced iron of the concentrate (from 5,95% Fe_2O_3 to 1,6%) and considering that whole P of the concentrate would be reduced and dissolved in reduced iron, one would expect a Fe-P alloy with 15,2% of P. This P content is closed to the P analyzed in most Fe-P particles.

The low tin content in the Fe-P particles, of the acceleration step, compared with tin content in Fe-P particles of the initial step, confirm the hypotheses that Sn oxide was reduced preferentially in earlier steps, being diluted by a more intense reduction of Fe

and P in later step. Probably, the earlier Sn oxide reduction occurred due to its low thermodynamic stability.

It can still mentioned that the majority of oxides reduced are porous, resulting in low resistance to the inlet reducing gas or to the outlet gas. In addition, it was not observed topochemical evidences, for example, an iron layer over the iron oxide particles. Moreover, the reduction occurred randomly in iron and phosphorus oxides. Therefore, it is possible that the chemical reactions are prevailing over the diffusion. Based on this hypothesis, some of the reduction reactions could be the controlling step of the overall reaction, or the boudouard reaction could be the controlling step, if it was slower.

Considering the results of the acceleration period, the best fitting with kinetic expressions was obtained adopting the equation representing a first-order reaction [6].⁽²⁾

$$k t = - \ln (1-f) \quad [6]$$

Where k is the kinetic constant; t is the time and f is the reacted fraction of carbon.

This best fitting is in agreement with the microstructural evaluation, which showed that diffusion barriers were not critic.

Figure 8(a) represents plots of $-\ln(1-f)$ versus reaction time for the experimental results shown in Figure 2. The values of the kinetic constants for each temperature were taken as the slopes of the straight lines. Based on these values an Arrhenius-type plot of $\ln k$ versus $1/T$ was constructed, as shown in Figure 8(b). The value of the apparent activation energy calculated from this plot was $296,3 \pm 29$ kJ/mol with 95% confidence interval for a coefficient of determination of 0,9904.

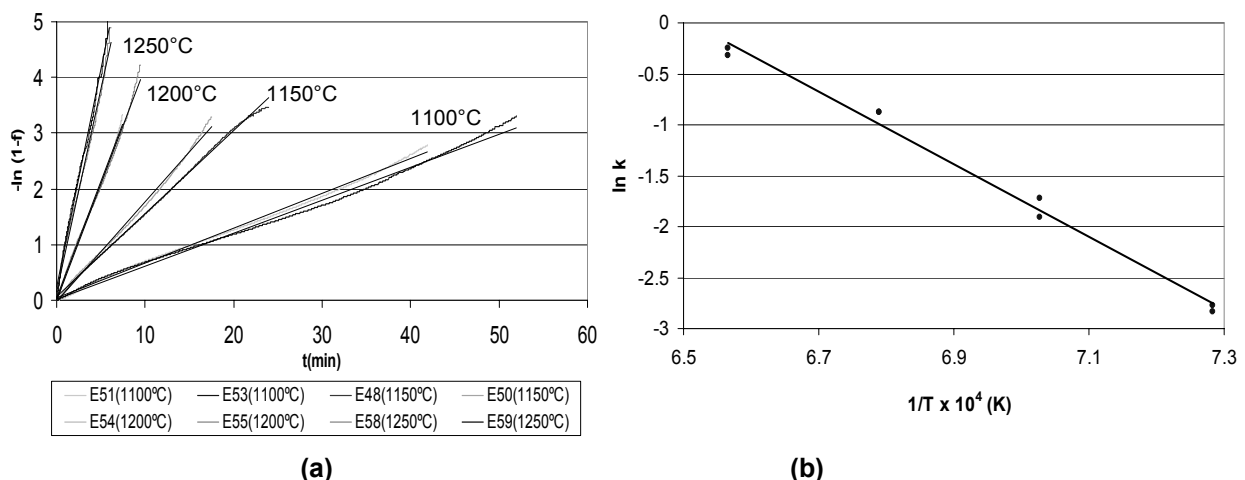


Figure 8. (a) Plot of $-\ln(1-f)$ versus time for self-reducing briquettes with graphite (1,86%C) -325#. **(b)** Plot of $\ln k$ versus $1/T \times 10^4$ for self-reducing briquettes with graphite (1,86%C) -325#.

This value is in the range of apparent activation energy for Boudouard reaction reported in the literature, which is between 251 and 359,5 kJ/mol.^(4,6,10,11) This range is closed to the range found in the literature for iron ore reduction in self-reducing pellets, where the step controlling was the Boudouard reaction.

The kinetic constant was also increased by addition of iron powder or Fe-P powder to the briquette mixture. This is an additional indication of the Boudouard reaction as controlling step of the overall reaction, since it is known that the Boudouard reaction is catalyzed by iron powder presence.⁽⁶⁾ These additions also practically eliminated the induction period. Details of this effect will be presented in future and it can be found in reference 2.

3.2 Effect of Graphite Particle Size

Figure 9 shows the effect of the particle size of the graphite on the reduction rate at 1150°C.

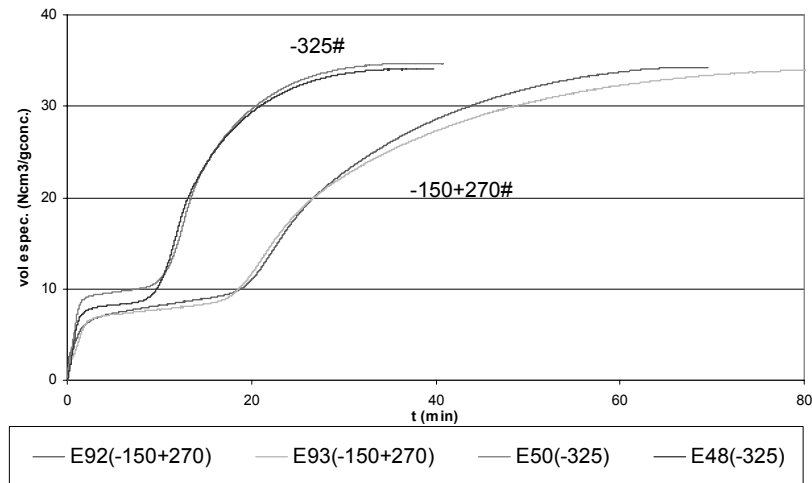


Figure 9. Effect of the graphite particle size on the reaction rate at 1150°C.

In this figure, it can be observed a decreasing of reaction rate when coarser graphite particles were adopted. This effect is an additional possible evidence of Boudouard reaction as controlling step. This same effect was observed by Rao et al.⁽¹⁰⁾ and Fruehan et al.⁽⁵⁾ in the iron ore or iron oxide reduction in self-reducing pellets, when the Boudouard reaction was considered as the controlling step of the overall reaction. Based on experiments carried out at different temperatures, it was constructed an Arrhenius-type plot of $\ln k$ versus $1/T$, as shown in figure 10. The value of the apparent activation energy calculated from this plot with graphite -150+270# was $285,3 \pm 65$ kJ/mol with 95% confidence interval for a coefficient of determination of 0,9738, which is closed to the value obtained with graphite -325#. Therefore, the use of coarser graphite caused a decreasing on the reaction rate; however it was not observed any mechanism changing.

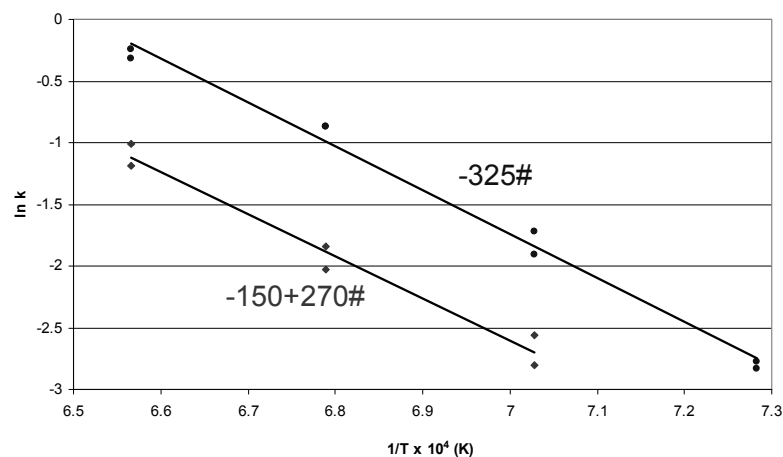


Figure 10. Plot of $\ln k$ versus $1/T \times 10^4$ for self-reducing briquettes with graphite (1,86%C) -325# and -150+270#.

4 CONCLUSIONS

- It was observed a significant effect of temperature on the reduction reaction rate of P, Pb, Sn and Fe oxides of the niobium concentrate.
- Experiments carried out at low temperatures showed a step where the reduction rate was very slow. This step, called induction period, is characterized by a nucleation period, where the first metallic nuclei were formed.
- The faster reduction rate occurred during the acceleration step, which was characterized by an increasing of number of metallic nuclei, where the majority of Fe-P (10-15%P) particles were formed.
- It was observed that the tin was reduced in the earlier steps, producing Fe-P particles with high Sn content. However, the tin content in Fe-P particles was lower than 2,5% at the end of experiments.
- It was observed that regions of calcined concentrate, rich in P and Al (probably gorceixite mineral after calcination) were transformed in a region rich only in aluminum and oxygen (probably alumina), showing that the main source of P was, probably, a phosphate with low thermodynamic stability, probably an aluminum phosphate, as shown by thermodynamic evaluation.
- Based on experiments carried out with graphite -325# as reducing agent, it was obtained an apparent activation energy of $296,3 \pm 29$ kJ/mol with 95% confidence interval.
- It was observed a decreasing of reaction rate when coarser particles of graphite were adopted. The apparent activation energy of $285,3 \pm 65$ kJ/mol was obtained with graphite between 150 and 270 mesh.
- The effects of temperature and particle size of graphite and the obtained value for apparent activation energy, indicate the Boudouard reaction as controlling step of the overall reaction of carbothermic reduction of Niobium concentrate between 1100 and 1250°C, using graphite as reducing agent to promote the reduction of iron and the impurities P, Pb and Sn.

Acknowledgements

The authors are grateful to the support of Companhia Brasileira de Metalurgia e Mineração – CBMM.

REFERENCES

- 1 SOUSA, C. A. F. The Evolution of FeNb Manufacturing. **Proceedings of the International Symposium Niobium 2001**. Orlando, USA. Dec 2-5, 2001, P 89-104.
- 2 FERREIRA NETO, J. B. Refino de Concentrado de Nióbio Através de Redução Carbotérmica. Doctor Thesis, Escola Politécnica da USP, São Paulo, Brazil. 2002 (223 p)
- 3 MOURÃO, M.B. Análise do Processo de Redução de Minério de Ferro por Carbono na forma de pelotas Auto-Redutoras. 1988, 191p. Doctor Thesis. Escola Politécnica da Universidade de São Paulo.
- 4 RAO, Y. K. Catalysis in extractive Metallurgy. **Journal of Metals**. p. 46-50, July 1983.

- 5 FRUEHAN, R.J. The Rate of Reduction of Iron Oxides by Carbon. **Metallurgical Transactions B**, Warrendale, v. 8B, p. 279-286, June 1977.
- 6 TURKDOGAN, E.T.; VINTERS, J.V. Catalytic Oxidation of Carbon. **Carbon**, Oxford, v.10, p.97-111, 1972.
- 7 AJERSCH, F. Chemical and Physical Characteristics Affecting the Reduction Kinetics of Iron Oxide Pellets with Solid Carbon. **Canadian Metallurgical Quarterly**, Oxford, v.26, n.2, p.137-144, 1987.
- 8 GUPTA, S.K.; RAJAKUMAR, V.; GRIEVESON, P. Kinetics of reduction of Ilmenite with Graphite at 1000 to 1100°C. **Metallurgical Transactions B**, Warrendale, v.18B, p.713-718, Dec. 1987.
- 9 HINO, M.; NAGASAKA, T.; BAN-YA, S.; Activity of P in α -Fe and Phase Diagram of Fe-Fe₂P System above 1273 K. **Z. Metallkd**, v.88, p.938-944, 1997.
- 10 RAO, Y. K. The Kinetics of Reduction of Hematite by Carbon. **Metallurgical Transactions**, Warrendale, v. 2, p. 1439-1447, May 1971.
- 11 TURKDOGAN, E.T.; VINTERS, J.V. Effect of Carbon Monoxide on the rate of oxidation of charcoal, graphite and coke in carbon dioxide. **Carbon**, Oxford, v.8, p.39-53, 1970.